J. Fluid Mech. (1977), *vol.* 83, *part* 4, *pp.* 673–693
Printed in Great Britain

Pattern-recognized structures in bounded turbulent shear flows

By JAMES M. WALLACE,
Department of Mechanical Engineering, University of Maryland, College Park
ROBERT S. BRODKEY
Department of Chemical Engineering, The Ohio State University, Columbus
AND HELMUT ECKELMANN
Max-Planck-Institut für Strömungsforschung, D3400 Göttingen, Germany

(Received 7 July 1976)

It is now well established that coherent structures exist in turbulent shear flows. It should be possible to recognize these in the turbulence signals and to program a computer to extract and ensemble average the corresponding portions of the signals in order to obtain the characteristics of the structures. In this work only the u-signal patterns are recognized, using several simple criteria; simultaneously, however, the v or w signals as well as uv or uw are also processed. It is found that simple signal shapes describe the turbulence structures on the average. The u-signal pattern consists of a gradual deceleration from a local maximum followed by a strong acceleration. This pattern is found in over 65 % of the total sample in the region of high Reynolds-stress production. The v signal is found to be approximately 180° out of phase with the u signal. These signal shapes can be easily associated with the coherent structures that have been observed visually. Their details have been enhanced by quadrant truncating. These results are compared with randomly generated signals processed by the same method.

1. Introduction

As a result of work over the last decade, there is now an abundance of evidence for the existence of what have come to be known as coherent structures in turbulent shear flows. Although some of the characteristics of these structures have been determined, there is still much that is unknown about their nature and origin. Two recent review papers provide a thorough description of the development of this research: Laufer (1975) discusses both bounded and unbounded turbulent shear flows while Willmarth (1975) reviews the work on the structure of turbulence in boundary layers. The interest generated in this problem has recently been further attested to by an international colloquium at Southampton, an account of which has been published by Davies & Yule (1975). With these recent surveys readily available, it should not be necessary to repeat a review of this literature here; only the papers of immediate pertinence to this work will be cited.

This paper describes the use of a pattern-recognition technique for analysing turbulent velocity signals in order to detect and describe the velocity-signal signatures

of coherent structures in a fully developed turbulent channel flow. We were convinced that, if indeed coherent structures do exist in the flow, their signatures should be recognizable in the velocity signals of a probe placed at a point in the flow. Why, then, has this been such an elusive problem? Part of the reason is the distribution of scales seen in the turbulent velocity signals. A flow structure passing a probe will only occasionally be intersected directly through its centre; often it will be intersected near an edge. In addition, structures will pass the probe at different stages of their lifetimes. For these reasons, wide distributions of both amplitudes and frequencies are seen in the velocity signals. A successful pattern-recognition technique must be able to detect this whole range of sizes and normalize them to obtain a meaningful average pattern.

After spending many hours studying the detailed shapes of time traces of the u, v and uv turbulence signals in the wall region, we became convinced that there is indeed a characteristic pattern that is related to the coherent-structure event sequence (see Kline *et al.* 1967; Corino & Brodkey 1969), and that its predominant feature occurs in the streamwise fluctuating velocity signal u. This feature is a weak deceleration of the flow seen as a small negative gradient in the u signal followed by a period of almost constant and relatively low velocity and then a strong acceleration of the flow characterized by a large positive gradient in the u signal. This kind of perturbation in the signal can occur during periods when the general amplitude of the streamwise velocity is at any level, relatively high, low or somewhere in between, compared with the mean. This means that these perturbations, which were found to vary in scale over about half an order of magnitude, were superimposed on perturbations of much larger scale and lower frequency. Our objective was to see how much of the total signal sample contained this pattern and what kinds of pattern were occurring simultaneously in the v, w, uv and uw signals. We wanted, of course, finally to know whether these characteristic patterns would give some insight into the nature of the coherent motions.

The data for a fully developed turbulent channel flow used in this work are the same data as were analysed and reported by the authors in Brodkey, Wallace & Eckelmann (1974). The details of the oil channel flow and the instrumentation with which the data were taken have been described in that paper, by Eckelmann (1970, 1974) and by Wallace, Eckelmann & Brodkey (1972). Some of the most important features will be repeated here for the convenience of the reader. The data were obtained in a fully developed channel flow with a pure paraffin-based oil as the fluid. The Reynolds number of the flow based on the centre-line velocity of 21 cm/s and the channel width of 22 cm was 7700. The kinematic viscosity ν of the oil is 0·06 cm^2/s. At this Reynolds number, the thickness of the viscous sublayer given by $u_\tau y/\nu = 5$, where the friction velocity u_τ is 1·06 cm/s, is about 2·8 mm, allowing good probe resolution. The X-probe used to obtain the u and v turbulent velocity components was a standard TSI Model 1241-20W with quartz-coated film sensors 1 mm long and a spacing between the sensors of 0·7 mm. This separation is somewhat smaller than the Kolmogorov scale, which is about 1 mm. Data for the u and w components taken by Kreplin (1976) in the same channel under the same flow conditions using a V-probe were also analysed. This probe was self-made and had sensors which were of the same type as those for the X-probe and were 1 mm long. Pairs of constant-temperature anemometers and linearizers were used to operate the probes. For the overheat ratio of 1·01 used in this work, the minimum upper frequency limit of the probes at any of the measurement locations in the

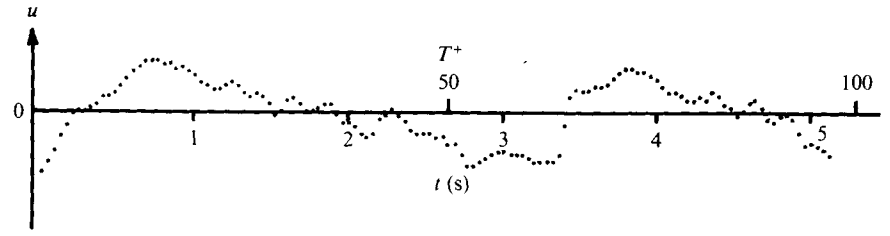

FIGURE 1. The characteristic pattern recognized in the digitized u signal ($T^+ = u_\tau^2 t/\nu$).

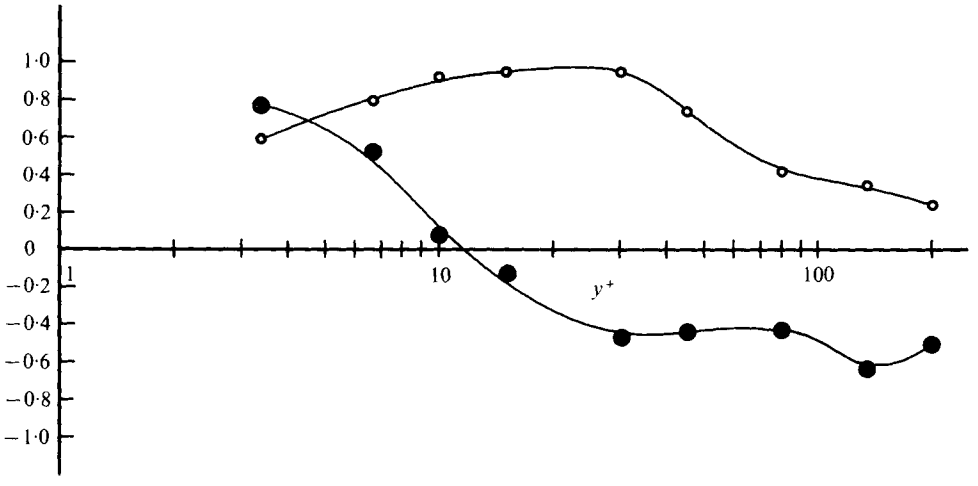

FIGURE 2. The skewness factors of u and du/dt. ○, du/dt; ●, u.

flow was 525 Hz. Since the highest frequency occurring in this low Reynolds number flow is about 20 Hz, the frequency response of the probes is not a problem.

The linearized signals were digitized at a rate of 50 samples/s and stored on the magnetic disc of a PDP-15 computer. They were subsequently transferred to magnetic tape so that the analysis reported here could be done on a UNIVAC 1108 computer.

2. The recognized pattern

A segment of a u signal containing the characteristic pattern is shown in figure 1. This is a segment of the raw digitized data (every second digitized point is shown in the figure). One sees immediately the strikingly characteristic weak deceleration and strong acceleration. The same characteristic of the u signal was found by Blackwelder & Kaplan (1972) to occur when turbulence-generating structures known as 'bursts' were detected at $y^+ = 15$. To confirm that this was really characteristic of the entire signal during much of the time, we looked at the skewness factor $S = \overline{(du/dt)^3}/[\overline{(du/dt)^2}]^{\frac{3}{2}}$ of the time derivative of the u signal. The time derivative was obtained numerically as suggested by Hershey, Zakin & Simha (1967) by fitting a second-degree polynomial to a moving window of five digital points and determining the slope at the centre of the window. The window is shifted one point forwards each time a new data point is

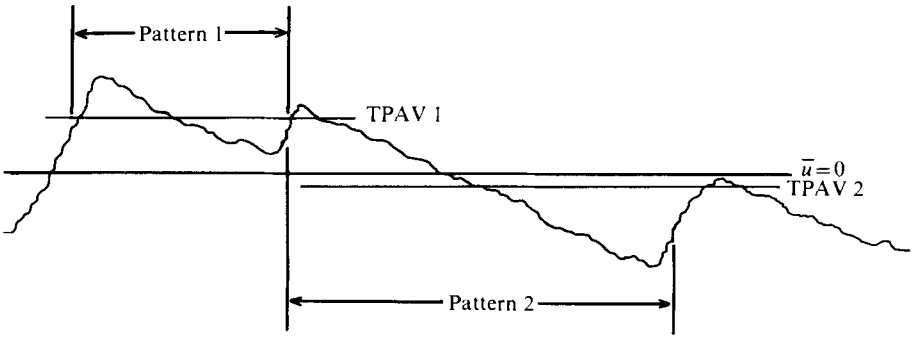

FIGURE 3. Sketch illustrating the use of TPAV in the recognition program.

called up. The equation suggested in the reference cited which was used to determine the derivative is

$$du(n)/dt = [-2u(n-2)-u(n-1)+u(n+1)+2u(n+2)]/10\,\Delta t,$$

where $u(n)$ is the nth digitized value of u and Δt is the inverse of the sampling rate.

The skewness S is highly positive from the wall to the centre-line of the channel as seen in figure 2. This indicates that there are many more occurrences of large positive values of du/dt than of large negative values. It is contrasted with the skewness factor of the u signal itself, which changes sign at $y^+ \sim 12$. This was strong quantitative evidence that our visual observation about the shape of the u signal was correct.

The skewness S has been measured in a nearly isotropic turbulent field downstream of a grid by Batchelor & Townsend (1947) and by Frenkiel & Klebanoff (1971). For $20 \lesssim R_\lambda \lesssim 60$, where $R_\lambda = (\overline{u^2})^{\frac{1}{2}}\lambda/\nu$ and λ is the Taylor microscale, Batchelor & Townsend found S to be about 0·4 whereas Frenkiel & Klebanoff found values of about 0·5 at $R_\lambda \sim 40$ and 0·4 at $R_\lambda \sim 60$. In the turbulent channel flow reported here, S is greater than 0·9 in the region $10 \lesssim y^+ \lesssim 30$, where the Reynolds stress and the turbulence production have pronounced maxima, and the patterns described in this paper display their most distinct characteristics. In this region of the channel flow, $90 \lesssim R_\lambda \lesssim 140$. Panchev (1971, p. 183) has shown that positive values of S are associated with the production of vorticity by stretching of vortex lines. Thus this region in the channel flow is also a region of high vorticity production. Panchev defined S in terms of spatial derivatives, which simply changes the sign of S as used here.

3. The pattern-recognition technique

Several ideas were incorporated in the computer algorithm designed to recognize the u velocity patterns. Since we believed the pattern to be a perturbation about a very low frequency variation, it was decided to look at the fluctuations within a given pattern about its own average, i.e. the average taken over the length of the pattern. The pattern length for this short-time temporal average (hereafter referred to as TPAV) was taken to be the period from one maximum in du/dt to the next. TPAV is thus defined as

$$\text{TPAV} = \frac{1}{M-m}\sum_{n=m}^{M} u(n),$$

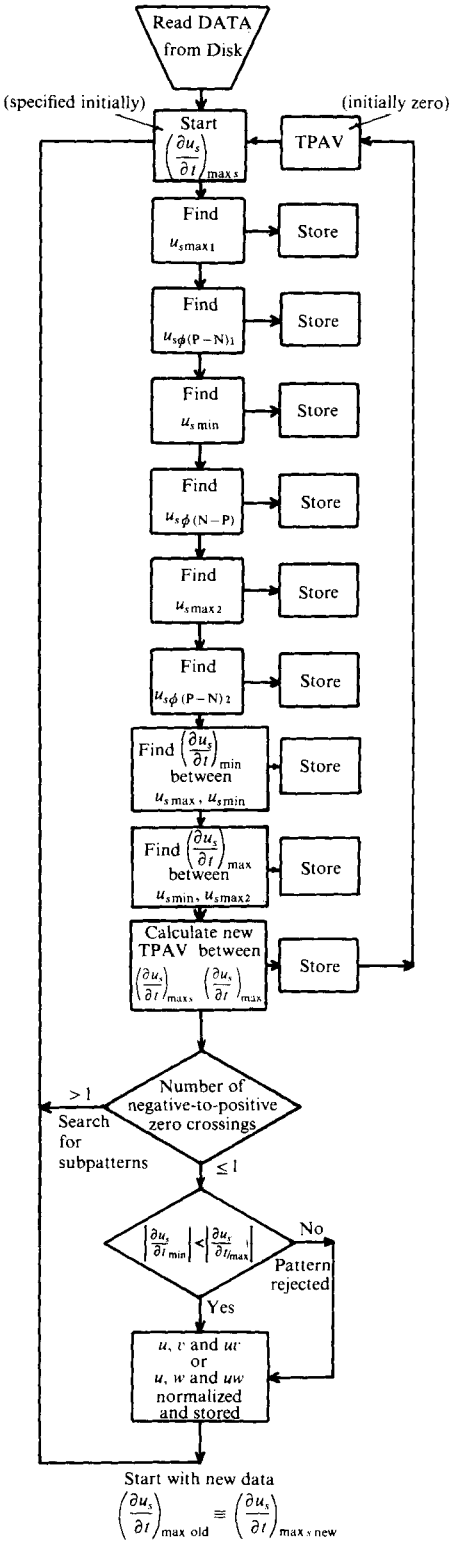

FIGURE 4(*a*). For legend see next page.

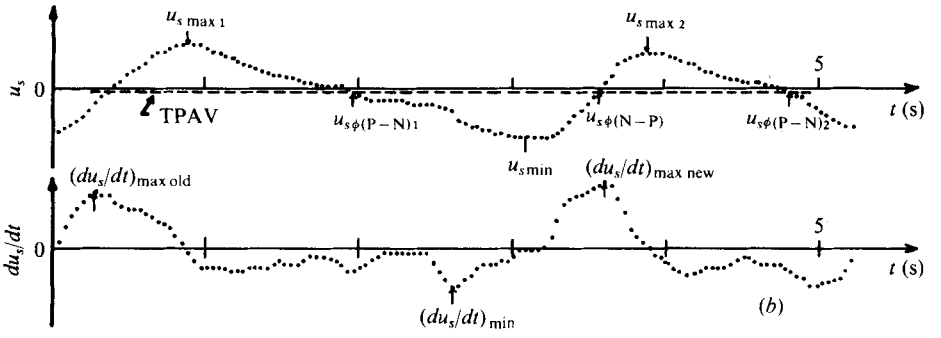

FIGURE 4. (*a*) Flow diagram showing the operation of the recognition program. (*b*) The smoothed u and du/dt signals, illustrating the operation of the recognition program.

where m is the first and M is the last point in the pattern. TPAV was subtracted from the u signal to obtain the fluctuating u velocity component used in the pattern-recognition scheme. Figure 3 shows a sketch of a segment of u signal that is recognized as two patterns using the temporal-average idea. If the long-time mean velocity $\bar{u} = 0$ had been used, these patterns would have been missed.

Another idea incorporated in the algorithm is a comparison of the slope of the u signal during its deceleration with the slope during its acceleration. It was our contention that the deceleration phase of these patterns is weak while the acceleration phase is quite strong. For most of this work we simply required that the positive slope be greater in absolute value than the negative slope. The advantage of this as a criterion is that no arbitrarily chosen discriminator level is required. We later ran tests where we required the positive slope to be two and three times greater than the negative slope; these tests are described in §4.2.

The digitized u signal was also smoothed for the recognition using a simple 11 point (0·22 s) moving-window average to eliminate fluctuations of a scale much smaller than those we were attempting to recognize. Each point in the smoothed signal, centred in the window, is the average of the points within the window length. This smoothed signal was used only for the recognition process; the unsmoothed data were used for the ensemble-averaging process described later. We were concerned that, if these fluctuations were left unsmoothed, we could have difficulties with the recognition algorithm, and we believed that the smoothing would not materially affect the results because there is virtually no energy contained in these data for frequencies above 5 Hz. The effect of smoothing, however, was tested by varying the window length from 5 to 23 points (0·1 and 0·46 s) and this will also be discussed later (§4.2). All the results reported in the next section were obtained using 11 point smoothing.

The recognition program functioned in the following manner (see figure 4). The digitized hot-film values from an X-probe were read from a magnetic disc and added and subtracted to obtain u and v. The product values uv were then formed and the recognition program begun. The program started at an arbitrary point in the data, and the value of TPAV was initially set at zero. The program marched through the data, finding the first maximum $u_{s\mathrm{max}1}$ in the smoothed u signal, the first positive-to-negative TPAV crossing $u_{s\phi(\mathrm{P-N})1}$, a minimum $u_{s\mathrm{min}}$, a negative-to-positive TPAV crossing $u_{s\phi(\mathrm{N-P})}$, the second maximum $u_{s\mathrm{max}2}$ and the second positive-to-negative TPAV crossing $u_{s\phi(\mathrm{P-N})2}$. It then went back and found the largest negative value

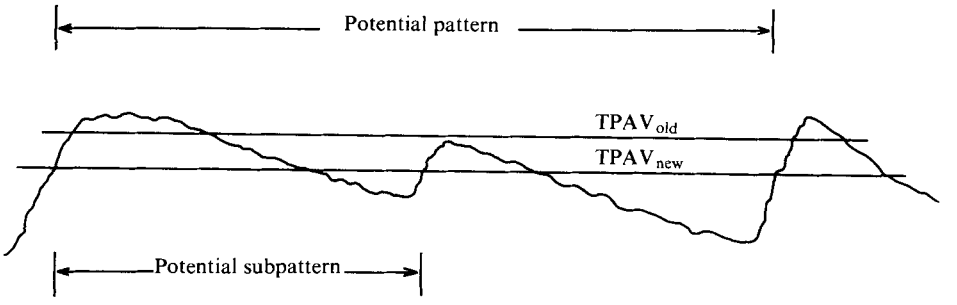

FIGURE 5. Sketch illustrating the iteration procedure in the recognition program for finding subpatterns.

$(du_s/dt)_{min}$ of the time derivative of the smoothed u signal between u_{smax1} and u_{smin} and the largest positive value $(du_s/dt)_{max}$ of the derivative signal between u_{smin} and u_{smax2}. TPAV for this potential pattern was found between the old and new positive derivative maxima and replaced the old TPAV, which for this first pattern was set at zero. It was then determined whether there was more than one negative-to-positive crossing of this new TPAV. If there was more than one, this was an indicator that there were potential subpatterns within this potential pattern. These subpatterns were then sought by starting again at the initial point using this new value of TPAV as the new initial TPAV. This iteration process is sketched in figure 5, which shows a subpattern that is initially missed by the recognition using the old TPAV but is then recognized after the negative-to-positive crossings have been sought using the newly calculated TPAV. When no or only one negative–positive crossing was found, after iterating to look for subpatterns if necessary, the potential pattern was tested using the slope criterion to classify it as either an accepted or a rejected pattern. If $|du_s/dt|_{max} > |du_s/dt|_{min}$, then the pattern was accepted; otherwise it was classified in the rejected category.

At this point the segments of the *unsmoothed* u, v and uv signals for the time interval of the pattern's occurrence were normalized to an arbitrarily chosen unit time interval and stored in reserved storage locations in the computer. This was done for both the accepted and the rejected patterns since we wished to study both. The unit time interval for normalization was taken as 120 points (2·4 s). Thus normalization compressed longer patterns and stretched shorter ones. As each new pattern was obtained and normalized, the points along its length were added to those previously stored for u, v and uv to obtain, eventually, an ensemble average. For the u signal, $U-\overline{U}$ was used, where $\overline{U}$ is the long-time mean; $UT-PAV$ was not used. Since squares or products with V are not involved, $U-TPAV$ and $U-\overline{U}$ have exactly the same shape. We chose to plot $u = U-\overline{U}$ in the figures as is conventionally done and show the mean for all events of TPAV on each figure. For the v signal, $\overline{V}$ is zero so $v = V$ was used. For the uv signal, $(U-TPAV)V$ was used rather than the conventional $uv = (U-\overline{U})v$. Clearly $(U-TPAV)v$ and $(U-\overline{U})v$ are not equal. Both were tried and we found that $(U-TPAV)v$ sharpened somewhat the shapes of the uv patterns. Throughout the text the notation uv will be used to indicate $(U-TPAV)v$. In the normalization, the minimum and maximum points of du_s/dt were always located at the 35th and 85th points along the 120 point time scale.

The recognition criteria and normalization technique predetermine the shape of the average recognized u patterns. The v and uv patterns have no criteria imposed on them which predetermine their shape. This is the significance of the procedure. It educts the features of the v and uv signals occurring during a selected feature in the u signal.

After the accepted or rejected patterns had been normalized and stored, the program searched for the next pattern, starting at the maximum in the slope using as the initial TPAV that of the pattern just analysed, and continued until 128000 data points of each of the u, v and uv data sets had been processed. Later the program was tested with much larger sample sizes, but 128000 points were found to be completely adequate.

4. Results

4.1. *Recognized u, v and uv patterns*

In figure 6, the normalized and ensemble-averaged patterns for u, v and uv are shown for 9 positions across the channel half-width. There are several characteristics that are noteworthy. Although the recognition technique required only that the maximum positive slope in the u pattern be larger in absolute value than the maximum negative slope, over most of the channel it is considerably larger. At $y^+ = 15$ and 30 the ratios are 1·9 and 1·7, respectively. The general shape of the u pattern is predetermined, and the v pattern must be generally out of phase with u since it is well known from previous work (e.g. Eckelmann 1970) that these two signals have a correlation coefficient of about $-0{\cdot}4$ over most of the channel half-width. However, the detailed features of the u and uv patterns are not known. In figure 6 we see positive–negative pulses in the v pattern which are largely out of phase with such pulses in the u pattern, resulting in the large negative pulses in the uv pattern. These are indicated as regions A and B at $y^+ = 30$ in the figure. Such pulses are the times when Reynolds stress is being produced and are associated with the ejection and sweep events in the event cycle described by Corino & Brodkey. The ejection events are characterized by energetic motion away from the wall of coherent regions of low streamwise velocity. Sweep events are of somewhat larger scale, have a streamwise velocity higher than the local mean, and move parallel to or slightly towards the wall. At $y^+ = 30$, ejections are the dominant producers of Reynolds stress. Nearer the wall, closer than the region where ejections principally originate, the sweep pulses are larger and are practically the only events occurring at $y^+ = 3{\cdot}4$.

Because the two patterns are not completely opposite in phase, there are points along the time axis when both are either positive or negative, giving rise to positive pulses in the uv pattern. This can easily be seen in the instantaneous uv signal but can even be seen here in these ensembled-averaged patterns because their lengths have been normalized. A region of this sort is indicated as C in the figure at $y^+ = 15$. These positive pulses are associated with the wallward interaction described by Wallace *et al.* as an interaction of the ejection and sweep events. They are motions of smaller scale than ejections and sweeps and are characterized by low velocity fluid which moves towards the wall. Here they occur at the beginning of the strong acceleration in the u pattern. The other type of interaction event (outward interaction), characterized by high speed fluid moving away from the wall, will be discussed in §4.3. Blackwelder

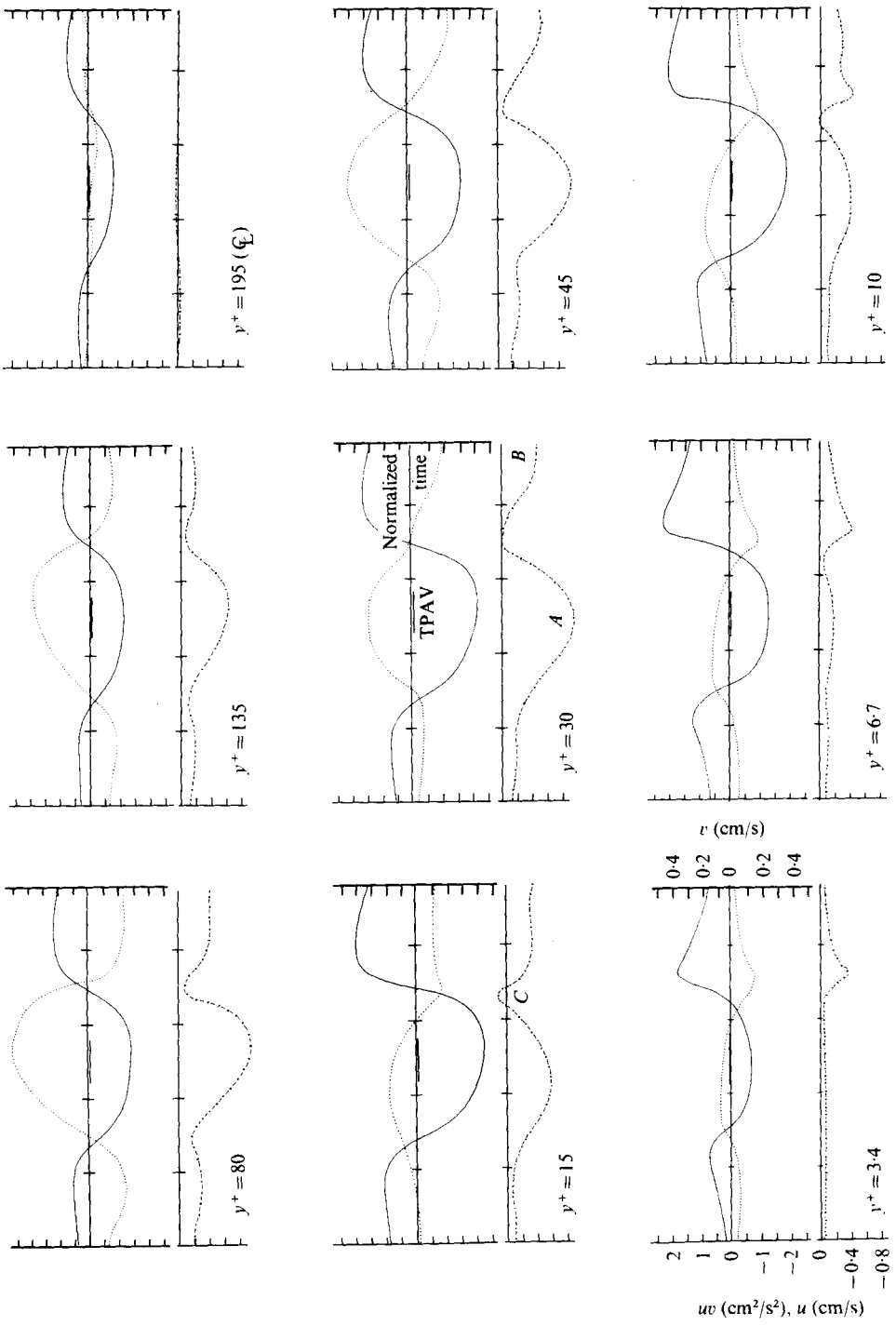

FIGURE 6. The normalized and ensemble-averaged u, v and uv patterns. ——, u; ·····, v; —·—, uv. (Scales identical at all y^+ values.)

y^+	$\bar{U}$ (cm/s)	Number of accepted patterns	Percentage of time in accepted patterns	T^* for accepted patterns	Number of rejected patterns	Percentage of time in rejected patterns	T^* for rejected patterns
3·4	4·02	502	55·9	5·45	458	44·1	4·70
6·7	6·91	635	63·3	4·87	453	36·7	3·96
10	10·14	846	65·4	3·77	504	34·6	3·35
15	12·24	966	65·5	3·31	586	34·5	2·88
30	15·49	1214	65·4	2·64	754	34·4	2·23
45	17·05	1303	59·7	2·23	908	40·3	2·17
80	18·95	1266	58·2	2·24	986	41·8	2·07
135	20·84	1203	54·7	2·22	1066	45·3	2·08
195	21·01	1264	51·5	1·99	1220	48·5	1·94

TABLE 1

& Kaplan (1976) have obtained strikingly similar results at $y^+ = 15$ for a uv signal conditionally averaged during periods of highly energetic fluctuations in the u signal at the same location. As noted in the introduction, they also found that the u signal, when conditionally averaged over these periods, exhibited the same characteristic weak deceleration and strong acceleration as are found in the present investigation. Their investigation was made in a boundary-layer flow with a momentum-thickness Reynolds number R_θ of 2550. An estimate of an equivalent R_θ for our channel flow is 430.

Several other interesting characteristics of these patterns can be seen in table 1. Near the wall and near the channel centre-line, the percentage of the total signal in the accepted patterns is more nearly equal to that in the rejected patterns. In the region $10 \leqslant y^+ \leqslant 30$, however, the accepted patterns account for over 65% of the total signal, or over 30% more than the rejected patterns. Since this is the region where the coherent bursting structures predominate, it appears that the patterns are closely related to the bursting process, and indeed we believe they describe the shape of these signals during this process. Also given in table 1 for each y^+ position are the number of patterns in each category and the average non-dimensional pattern length of occurrence $T^* = \bar{T}\,\bar{U}_{\mathbb{C}}/b$, where $\bar{U}_{\mathbb{C}} = 21{\cdot}01$ cm/s and the channel half-width $b = 11$ cm. These values agree well with the value of 3·0 given in Brodkey *et al.* Although the data used there and in this work are the same, the method of analysis is different. In Brodkey *et al.* the average period between occurrences of motion with $u < 0$ and $v > 0$ in the region $10 < y^+ < 45$ was used to obtain T^*. This value also agrees quite well with that obtained from data gathered from several sources by Laufer & Badri Narayanan (1971). Blackwelder & Kaplan (1976) found that the bursting sequence they detected at $y^+ = 15$ had an average duration of $\bar{T}\,U_\infty/\delta = 2{\cdot}8$, which also compares very well with the average pattern lengths in table 1, especially in the region $15 \leqslant y^+ \leqslant 30$. This further suggests that the two studies were observing the same bursting phenomena. They found that the detected bursting sequences occupy approximately 25% of their total sample. This is considerably less than the 65% found here using the pattern-recognition technique. As they point out, however, the number of bursts they detect depends on the threshold level of the detection criterion used. As will be seen in the next section, when we made the pattern-recog-

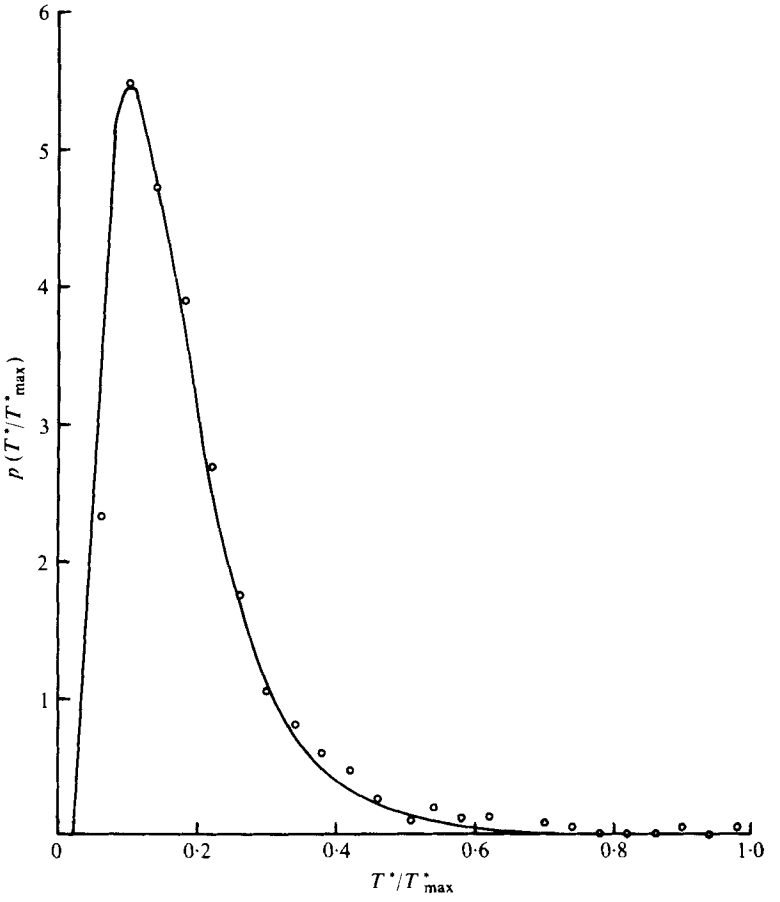

FIGURE 7. Probability density distribution of the normalized pattern length.

nition criteria more stringent the percentage of the total sample recognized was also considerably reduced.

Figure 7 shows the probability density distribution of T^* for the recognized accepted patterns at $y^+ = 30$. This distribution is very close to the lognormal distribution

$$p(T^*/T^*_{max}) = T^*_{max}/T^*\{[(2\pi)^{\frac{1}{2}}\sigma]^{-1}\exp\{-(2\sigma^2)^{-1}[\ln(T^*/T^*_{max}) - \ln(\overline{T}^*/T^*_{max})]^2\},$$

where T^*_{max}, the maximum non-dimensional pattern length occurring in the data set, is 13·1, σ, the standard deviation of T^*/T^*_{max}, is 0·59 and $\overline{T}^*/T^*_{max}$, the mean value, is 0·148. This distribution is shown as the solid line in the figure. The data points in the figure are the recognized pattern length distribution. The distribution is quite narrow, indicating the small range of scales in the flow. The ratio of the largest to the smallest scale is only about five.

An identical analysis to that described above was done for the u and w pair of signals using data obtained by Kreplin. As expected from symmetry considerations, the ensemble-averaged w and uw patterns were practically zero. This means that positive and negative w motions are equally probable during all phases of the recognized pattern in the u signal.

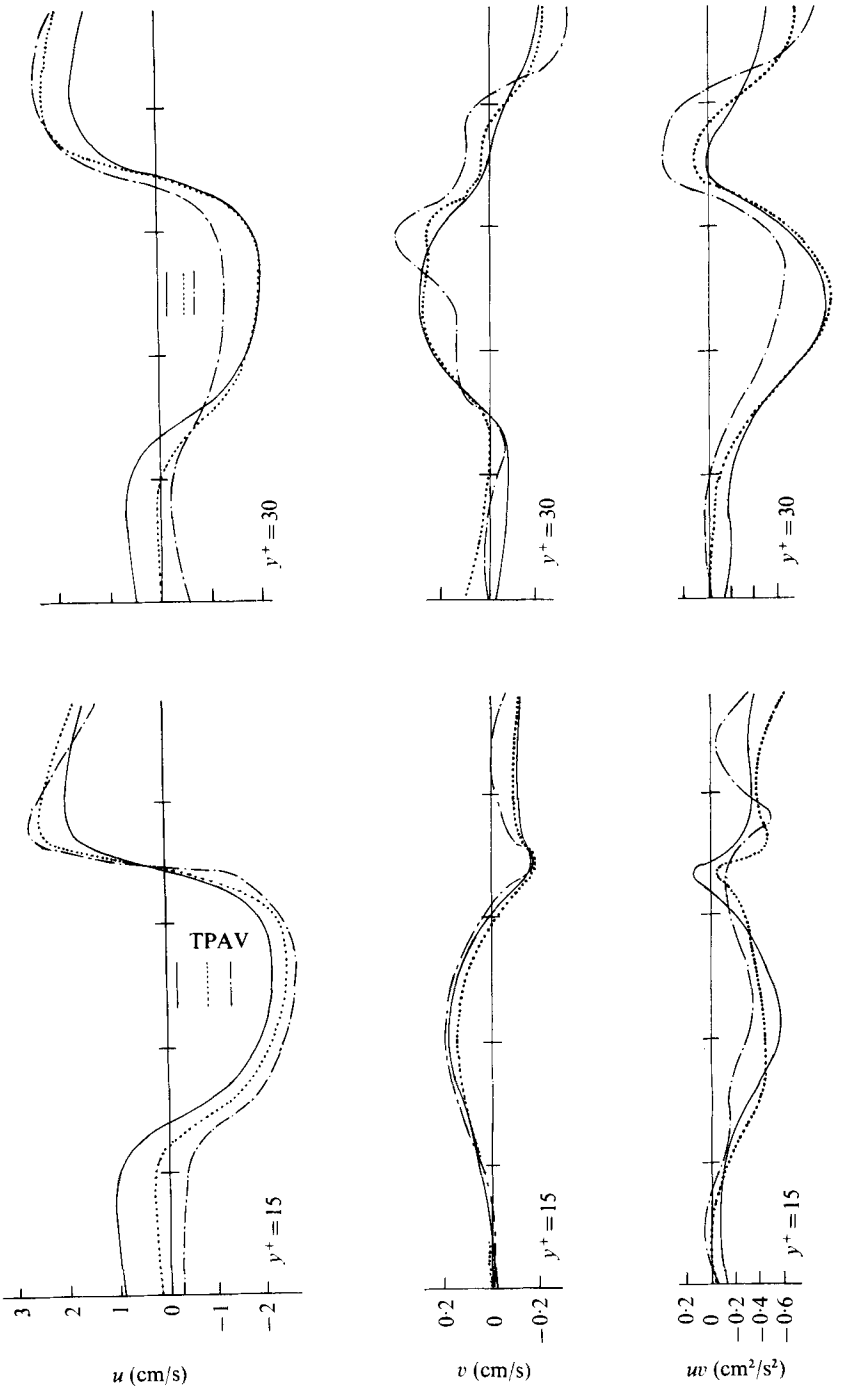

FIGURE 8. Patterns obtained using stronger slope comparison criteria. ——, 1:1; ·····, 2:1; —·—, 3:1.

4.2. *Testing of features of the recognition technique*

The data were analysed using 5 and 23 point smoothing for the moving-window average to test whether the degree of smoothing made any appreciable difference in the patterns recognized. The characteristic form of the patterns was unchanged. The only change that occurred when fewer points were used in smoothing was that slightly more patterns were detected because the higher frequency fluctuations were not being filtered out. Similarly, 23 point smoothing eliminated some of the patterns detected with 11 point smoothing, and thus the number of events detected was somewhat smaller. At $y^+ = 3{\cdot}4$, for example, 9 % more patterns were found using 5 point smoothing and 13 % fewer were found using 23 point smoothing. Clearly, doubling or halving the smoothing-window length does not appreciably affect the result.

The slope comparison criterion was varied by requiring that acceptable patterns have $|du_s/dt|_{\max} > 2|du_s/dt|_{\min}$ and $|du_s/dt|_{\max} > 3|du_s/dt_{\min}|$. These results are shown in figure 8 for $y^+ = 15$ and 30. The essential character of the patterns is not changed although, as would be expected, the characteristic features of the patterns are accentuated when stronger criteria are used. The curves are also much less smooth since with stronger criteria the number of patterns detected is correspondingly smaller. At $y^+ = 15$, 251 patterns occurring during 17·9 % of the total time were recognized with a 2:1 slope comparison criterion; for a 3:1 comparison these values were 77 and 5·3 %. At $y^+ = 30$ the values were 255 patterns over 12·8 % of the time at 2:1 and 51 patterns over 2·1 % of the time at 3:1. We also analysed the data without using any slope comparison criterion. The recognition criterion was in that case simply a recognition of the maximum–minimum–maximum sequence in the u signal; these results will be discussed in the next section.

Finally, two random signals were analysed with the pattern-recognition algorithm for comparison with the results for the wall shear-flow turbulence. These results will be discussed in §5.

4.3. *The u, v plane quadrant analysis*

To bring out further the characteristics of the coherent-motion event sequence, we incorporated an analysis technique first used by Wallace *et al.* and Willmarth & Lu (1972), namely that of truncating the u and v signals about their zero levels to obtain four classification criteria based on the pair of signs of u and v. We applied this truncation (about TPAV for the u signal and about zero for the v signal) to the pattern-recognized signal segments and normalized, stored and ensemble averaged u, v and uv for each of the conditions $u <$ TPAV, $v > 0$; $u >$ TPAV, $v < 0$; $u <$ TPAV, $v < 0$; and $u >$ TPAV, $v > 0$. The visually observed motions mentioned earlier which can be associated with these quadrants are ejections, sweeps, wallward interactions and outward interactions respectively. In figure 9 the recognized u patterns from figure 6 are shown for each of the nine y^+ positions together with the average patterns for each of the quadrant classes at each position. A number of interesting features can be observed. The most striking is the asymmetry of the wallward-interaction pattern in the region $10 \leqslant y^+ \leqslant 30$, and this is indicated by the letter D in the figure at $y^+ = 15$. The curves show a pronounced minimum in this region. The minimum occurs along the time axis at that point where the flow is beginning its strong acceleration, i.e. at

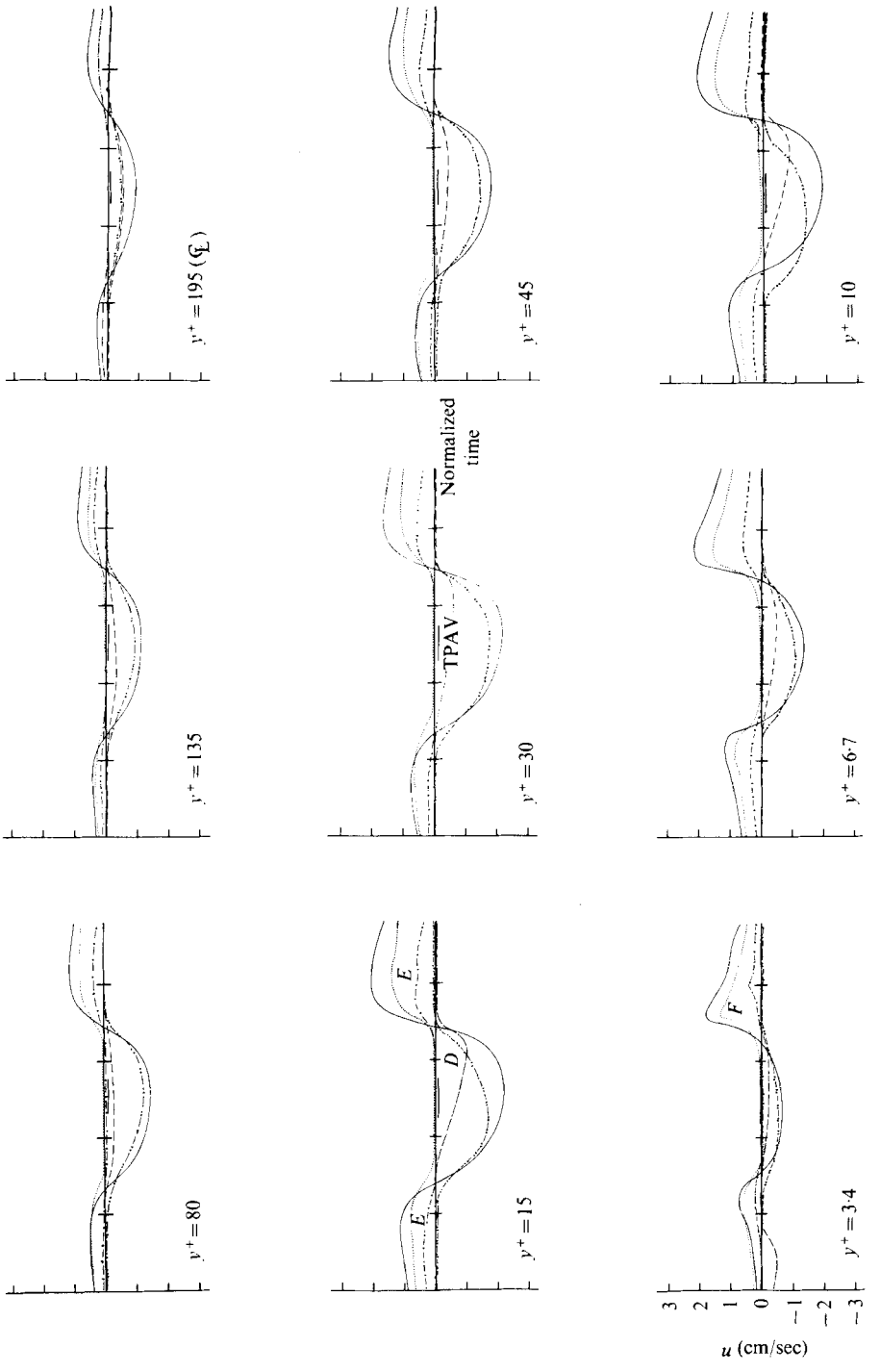

FIGURE 9. Quadrant analysis of u patterns (scales identical at all y^+ values). ·····, sweep; —··—, ejection; —·—, outward interaction; – – –, wallward interaction.

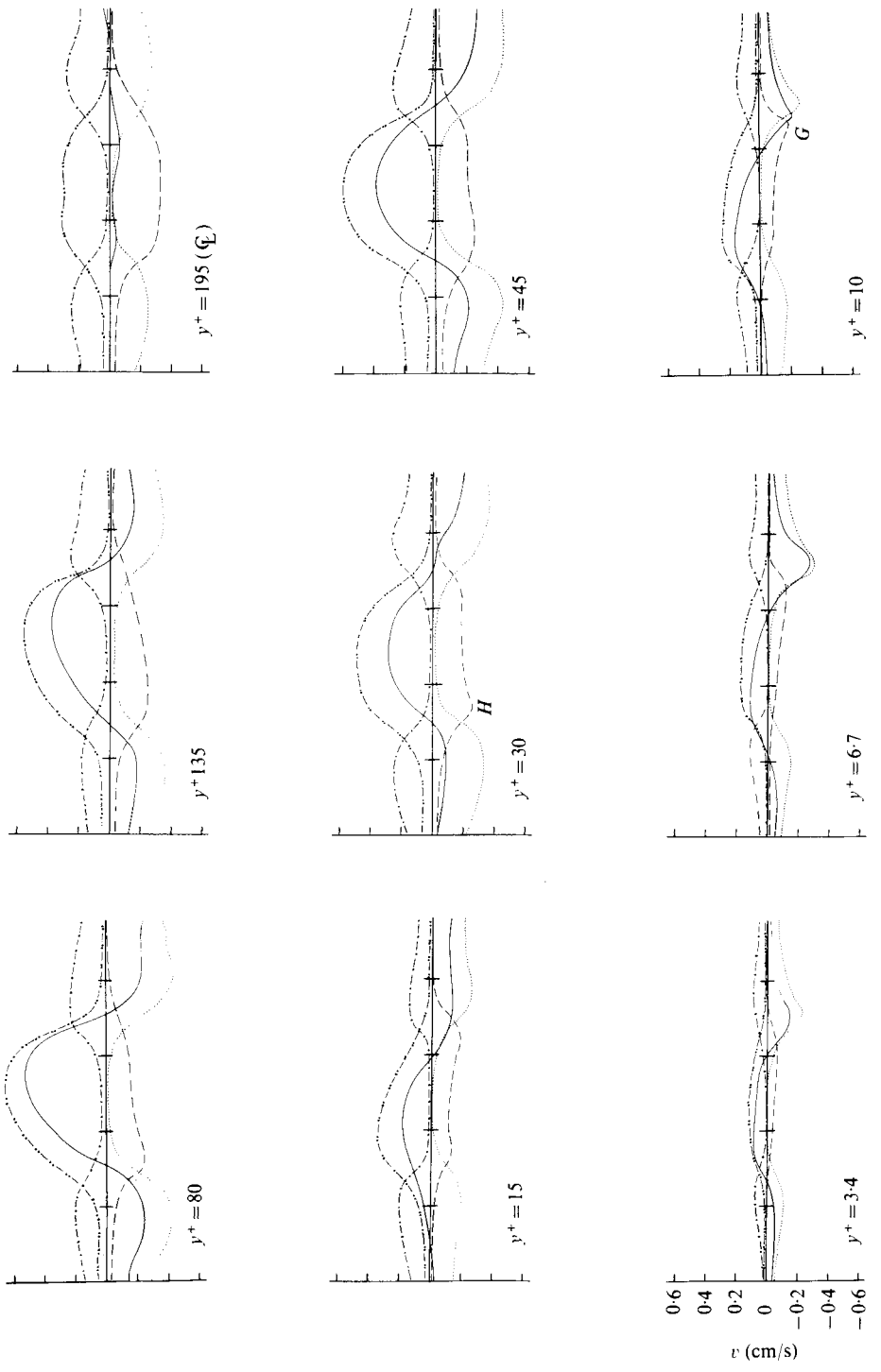

FIGURE 10. Quadrant analysis of v patterns (scales identical at all y^+ values). Notation as in figure 9.

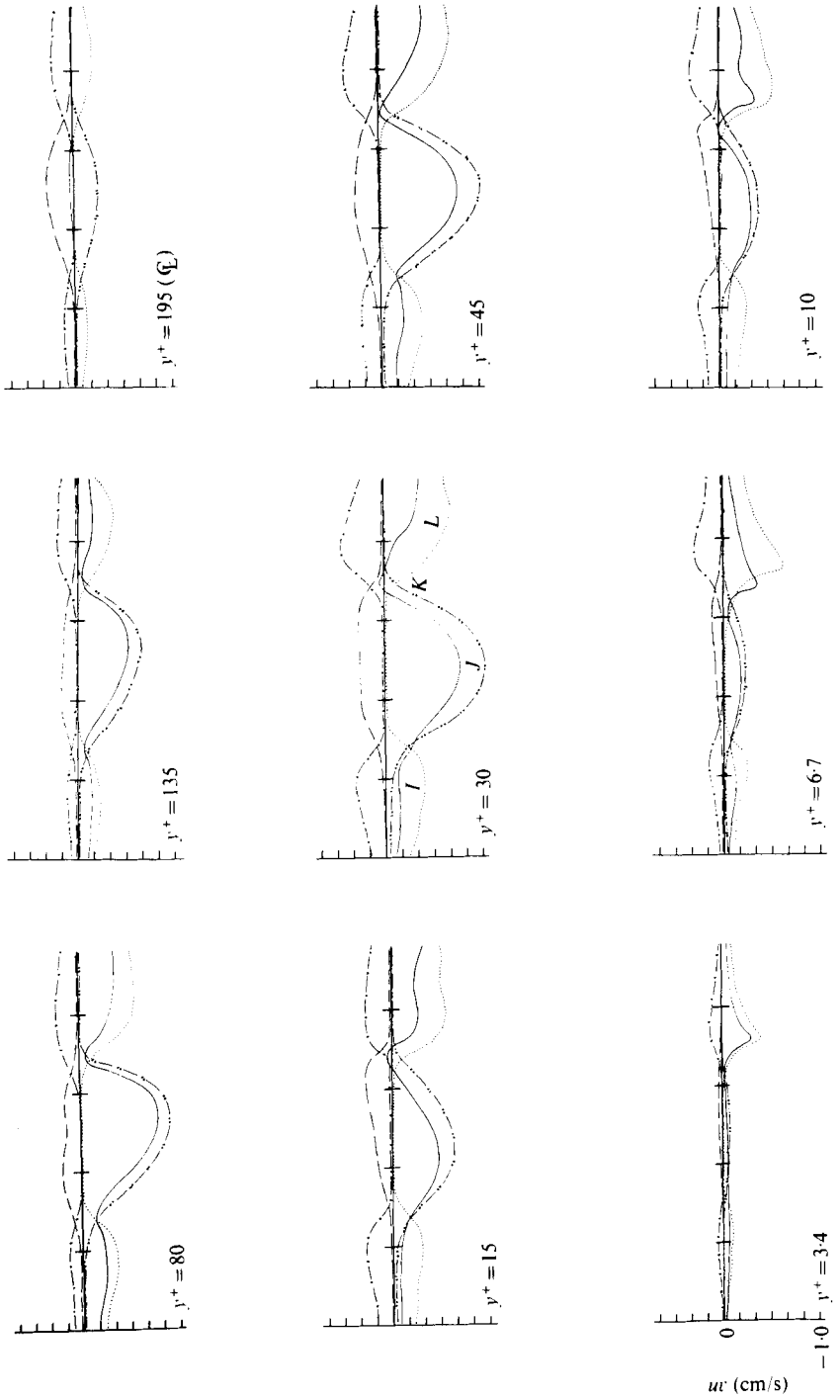

FIGURE 11. Quadrant analysis of uv patterns (scales identical at all y^+ values). Notation as in figure 9.

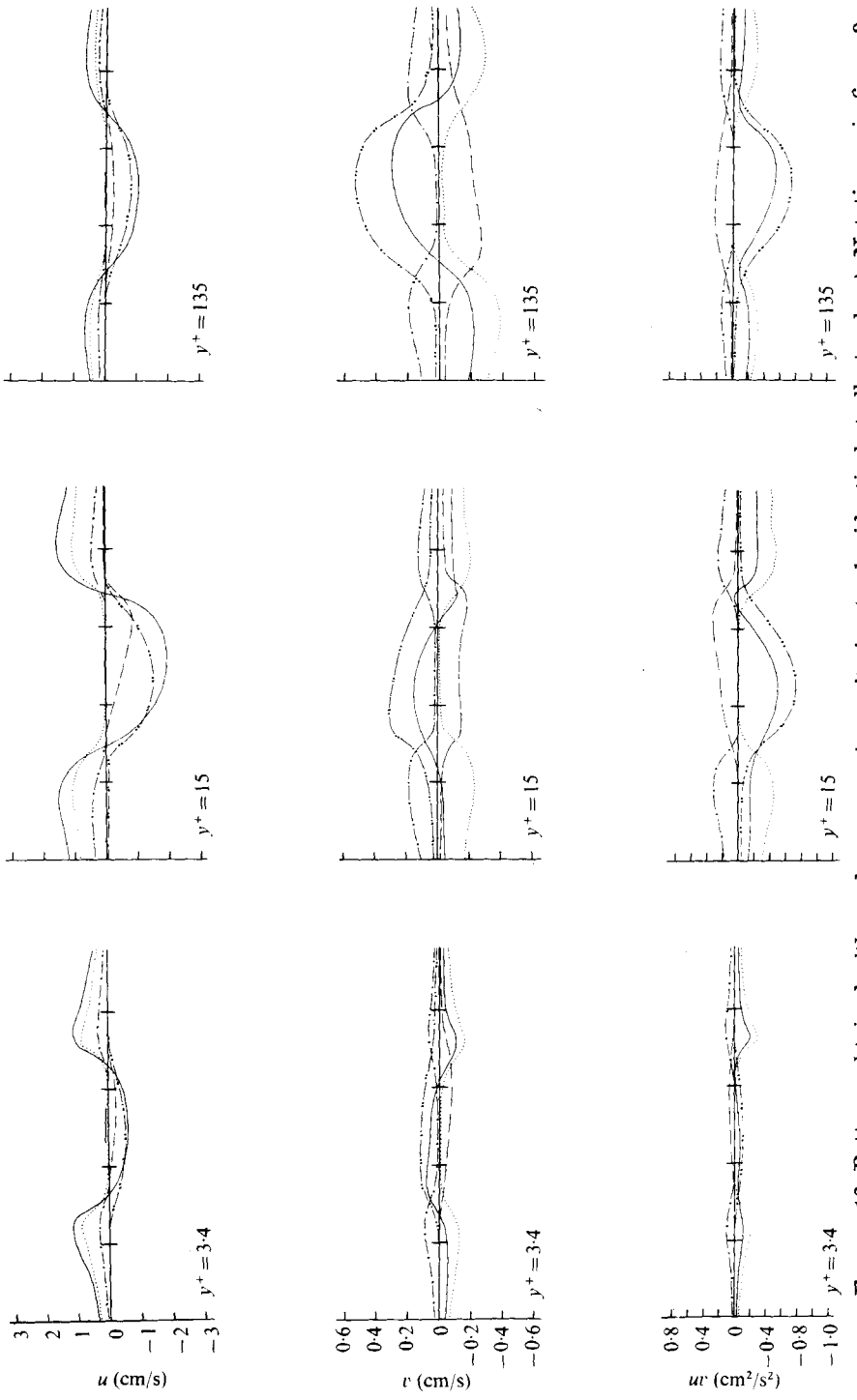

FIGURE 12. Patterns obtained with no slope comparison criterion (scales identical at all y^+ values). Notation as in figure 9.

the interface of the ejection and sweep events. This is exactly the place in the event cycle where this type of motion was observed in Corino's films (see Wallace *et al.*).

The outward-interaction patterns do not show this asymmetric character. They have shapes very similar to the sweep patterns as indicated by the letters *E* in the figure. This suggests that the interpretation of the nature of this motion in Wallace *et al.* and Brodkey *et al.* was incorrect. The outward-interaction motions now appear not to be an interaction between ejection and sweep motions, but rather to be sweeps with slight angles away from the wall. This type of sweep was not observed by Corino, although he did note that many sweep-type motions moved parallel to the wall. The wallward and outward interactions thus appear to be quite different kinds of motion.

Very close to the wall ($y^+ = 3{\cdot}4$), the sweep pattern has the largest amplitude and is the predominant motion (*F* at $y^+ = 3{\cdot}4$ in figure 9), which is again consistent with visual observations and the analysis of the total signal in §4.1. Ejections originate somewhat further from the wall and move outwards while sweep motions can and do come right up to the wall.

Figure 10 shows the v patterns displayed in the same fashion. Again the wallward-interaction pattern shows the most striking characteristics. Near the wall it has a minimum during the acceleration phase of the sequence (*G* at $y^+ = 10$ in figure 10) as it did for u. Beginning at $y^+ = 30$, however, this minimum shifts to the other side of the pattern (*H* at $y^+ = 30$ in the figure). In this region it is occurring during the deceleration phase. This is the first indication from these data that there is an essential difference between the coherent motions in the near-wall region and those further out, a point strongly emphasized by Nychas, Hershey & Brodkey (1973) and most recently by Sabot & Comte-Bellot (1976). The latter authors have evidence that the large-scale transverse vortices observed by Nychas *et al.* in the outer region of a boundary layer occur in a turbulent pipe or channel flow in the outer region on either side of the centre-line.

The *sequence* of coherent motion events may be seen most clearly in figure 11, particularly in the curves at $y^+ = 15$ and 30. In figure 11 the uv patterns have also been resolved into their four quadrant components. From left to right along the normalized time axis, there occur almost simultaneous sweep and interaction outward pulses (*I*) at $y^+ = 30$ followed by a strong ejection pulse (*J*), a wallward-interaction pulse during the high acceleration of the flow (*K*), and finally sweep and outward-interaction pulses again to begin the next cycle (*L*). This confirms the picture of the event cycle reported previously from visual studies and quantifies its characteristics.

As mentioned earlier, we averaged all the results, both those accepted and those rejected by the slope comparison criterion, into one average pattern for each position. This is in essence a pattern recognition with no slope comparison, i.e. one that recognizes simply a maximum–minimum–maximum sequence in the smoothed u signal. It might be expected that the end points of the recognized u, v and uv patterns would have the same average values when all the data for both accepted and rejected patterns were ensembled averaged together. This does not occur since the maximum and minimum slope points in the u patterns are matched and not the end points. Thus the data points to the left and right of these matched points can be averaged in two successive patterns at different locations relative to the end points. These patterns for $y^+ = 3{\cdot}4$, 15 and 135 are shown in figure 12. If this figure is compared with figures 9, 10 and 11 it is seen that the essential shape and character of the patterns are changed very little

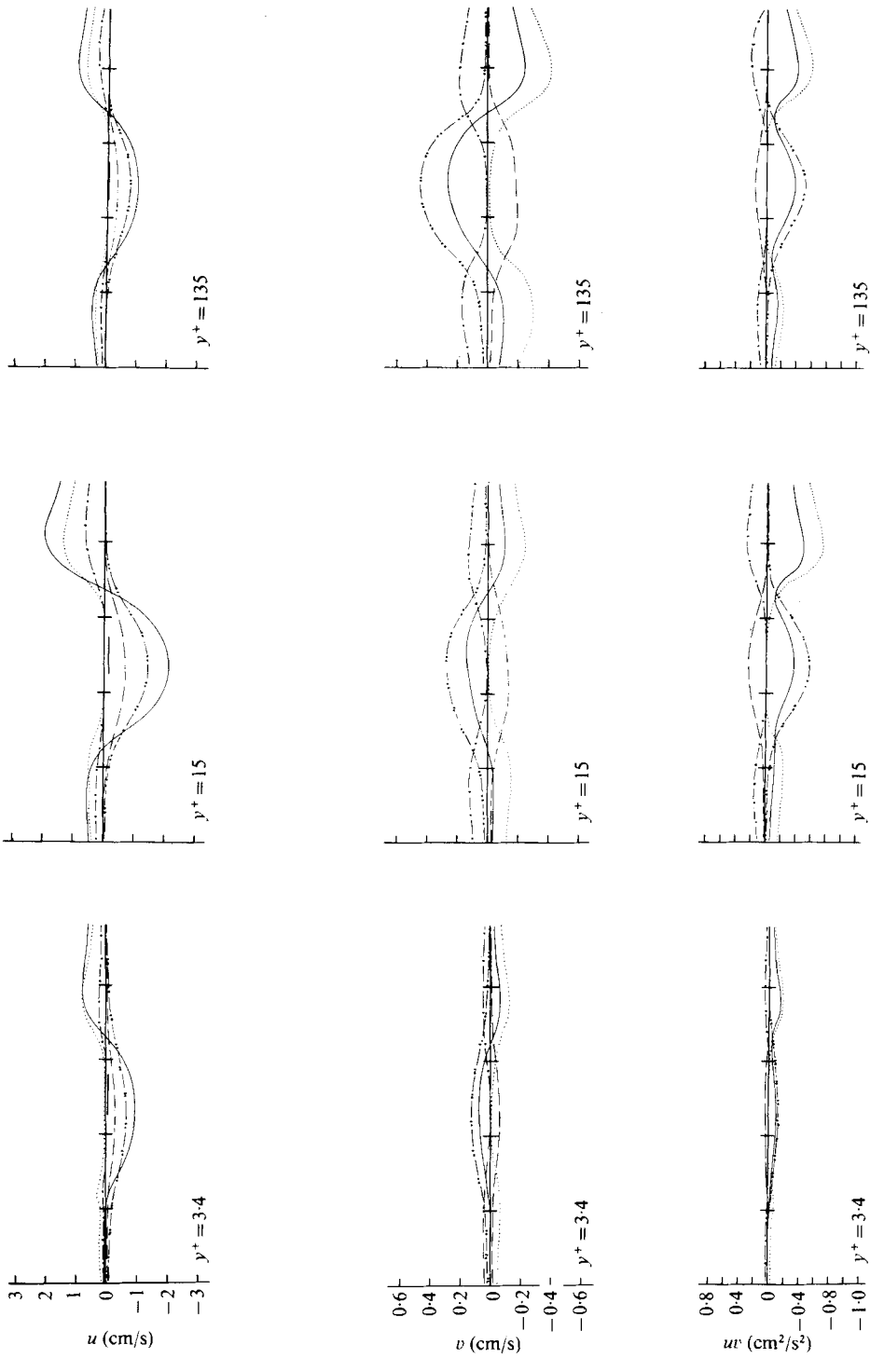

FIGURE 13. Patterns obtained from randomly generated data (scales identical at all y^+ values). Notation as in figure 9.

when this less stringent recognition criterion is used. The shapes are not quite as sharply defined as those obtained with the slope comparison criterion, but the essential characteristics are the same. This means that the entire data sample, and thus all the flow, can be characterized by these very simple wave forms.

5. Pattern recognition of randomly generated signals

We felt it essential to pattern recognize randomly generated signals to make a comparison with the results obtained from wall shear-flow turbulence. This comparison should demonstrate whether the distinguishing characteristics we observe in these patterns are produced by the analysis technique or whether they are real characteristics of the flow itself. Two statistically independent random signals x and y were generated by the computer and the random u and v signals were built from the functions

$$u = ax + y, \quad v = x + ay.$$

The r.m.s. amplitudes of x and y were specified such that the r.m.s. values of u and v would match the turbulence values at the respective y^+ positions. The frequency range of the channel-flow turbulence was also approximated by specifying the average zero-crossing rate of these random signals to be equal to that of the turbulence at the respective y^+ positions. Correlation coefficients $\overline{uv}/(\overline{u}^2)^{\frac{1}{2}}(\overline{v}^2)^{\frac{1}{2}}$ between 0 and 1 could be obtained by the selection of an appropriate value of $0 \leqslant a \leqslant 1$. The signals were first analysed with a correlation coefficient of zero. As anticipated, the ensemble-averaged v and uv patterns were zero across the entire normalized time interval. Then the random data were analysed using correlation coefficients equal to those for the actual turbulence data for y^+ positions of 3·4, 15 and 135. If these patterns, shown in figure 13, are compared with the corresponding curves in figures 9, 10 and 11, we see that the general shapes are similar, but that there are several striking differences in detail. The pronounced asymmetries in the wallward-interaction patterns at $y^+ = 15$ and 135 do not occur in these patterns for the randomly generated signals. At $y^+ = 3{\cdot}4$ the patterns of the randomly generated data show both weak ejection and weak sweep pulses in contrast to the single strong sweep pulse in the turbulence data.

The general features of the turbulence can thus be simulated with random data if the amplitude, frequency and correlation characteristics are matched. The details of the recognized structures are not found in the random data.

6. Conclusions

(i) The pattern-recognition technique described in this paper can detect and obtain ensemble averages of simple wave forms that are characteristic of the sequence of events producing Reynolds stress in the wall region of a bounded turbulent shear-flow.

(ii) The recognized u and v averaged patterns are approximately 180° out of phase.

(iii) In the region of high Reynolds stress, 65 % of the total signal contains the recognized pattern.

(iv) In this region, the acceleration within the u pattern is almost twice the deceleration.

(v) The wallward-interaction event occurs as the flow begins to accelerate and move towards the wall at the interface of the ejection and sweep events.

(vi) The outward-interaction event appears to be a sweep with a slight angle of inclination away from the wall.

(vii) A pronounced change in the character of the v pattern is seen beyond $y^+ = 30$, suggesting that the flow mechanism near the wall is different from that further out in the flow.

We should like to thank the director of the Max-Planck-Institute für Strömungsforschung, Prof. E.-A. Muller, who has encouraged and through the MPI supported the authors in various phases of this work, and Prof. W. W. Willmarth, who read the manuscript and made helpful suggestions. The data were obtained at the MPI and the computational analysis was also done there. The Ohio State University, Department of Chemical Engineering, supported J. M. Wallace as a Visiting Professor for the winter quarter of 1973 during the initial programming. R. S. Brodkey received the Alexander von Humboldt Foundation's Senior Scientist Award in 1975 during the latter phases of this work.

REFERENCES

Batchelor, G. K. & Townsend, A. A. 1947 *Proc. Roy. Soc.* A **190**, 534.

Blackwelder, R. F. & Kaplan, R. E. 1976 *J. Fluid Mech.* **76**, 89.

Brodkey, R. S., Wallace, J. M. & Eckelmann, H. 1974 *J. Fluid Mech.* **63**, 209.

Corino, E. R. & Brodkey, R. S. 1969 *J. Fluid Mech.* **37**, 1.

Davies, P. O. A. L. & Yule, A. J. 1975 *J. Fluid Mech.* **69**, 513.

Eckelmann, H. 1970 *Mitt. MPI Strömungsforsch. & AVA Göttingen*, no. 48 (available in English).

Eckelmann, H. 1974 *J. Fluid Mech.* **65**, 43.

Frenkiel, F. N. & Klebanoff, P. S. 1971 *J. Fluid Mech.* **48**, 183.

Hershey, H. C., Zakin, J. L. & Simha, R. 1967 *Ind. Engng Chem. Fund.* **6**, 413.

Kline, S. J., Reynolds, W. C., Schraub, F. A. & Runstadler, P. W. 1967 *J. Fluid Mech.* **30**, 741.

Kreplin, H.-P. 1976 *Mitt. MPI Strömungsforsch. & AVA Göttingen*, no. 63.

Laufer, J. 1975 *Ann. Rev. Fluid Mech.* **7**, 307.

Laufer, J. & Badri Narayanan, M. A. 1971 *Phys. Fluids* **14**, 182.

Nychas, S. G., Hershey, H. C. & Brodkey, R. S. 1973 *J. Fluid Mech.* **61**, 513.

Panchev, S. 1971 *Random Functions and Turbulence*. Pergamon.

Sabot, J. & Comte-Bellot, G. 1976 *J. Fluid Mech.* **74**, 767.

Wallace, J. M., Eckelmann, H. & Brodkey, R. S. 1972 *J. Fluid Mech.* **54**, 39.

Willmarth, W. W. 1975 *Adv. in Appl. Mech.* **15**, 159.

Willmarth, W. W. & Lu, S. S. 1972 *J. Fluid Mech.* **55**, 65.